Statistical Texture Recognition and Classification Using Variants of Local Binary Pattern

Shixuan Li

Abstract—Texture classification plays an essential role in different fields such as object recognition. One of the most widely used statistical methods is Local Binary Pattern (LBP). A large number of variants have been proposed, achieving competitive results in addition to computational efficiency. This study presents a new variant, Attractive-Repulsive Strength-Based LBP (ARSBLBP). Across four datasets with variations in angles, scales, and viewpoints, ARSBLBP achieves the best performance among eight LBP variants.

1 Introduction

In computational image processing, a texture can be viewed as a function defining the spatial variation of pixels' intensity, and a texture image is created when such variation follows a repeated pattern [1]. Texture classification plays an important role in various areas such as object recognition and defect detection.

Despite the increasing popularity of convolutional neural networks (CNNs), traditional methods are still prevalent, especially with small training sets and limited computational resources. One of the most widely used methods for extracting textural features is Local Binary Pattern (LBP). LBP was first proposed by Ojala et al. in [2] in 1996. Since then, it becomes the foundation of many state-of-the-art methods. LBP and its variants are not only used for texture classification, but also in many other fields including face recognition, iris recognition, and medical image analysis.

Hence, this study evaluates and compares a number of classic and novel LBP-based methods, using texture datasets of different characteristics. More importantly, in section 3.9, this study presents a new variant named Attractive-Repulsive Strength-Based Local Binary Pattern (ARSBLBP), achieving significantly better performance and computational costs.

2 Related Work

The foundational LBP in [2] is a gray-scale invariant method. For each local image patch, it binarizes pixel intensities by comparing them against the central pixel. The distribution of the resultant binary encoding then becomes a feature descriptor of each texture. However, LBP is not rotation-invariant. To address this major drawback, in [3], Ojala et el. proposed rotation invariant LBP (LBP^{ri}) and LBP^{riu2} for the detection of uniform pattern.

Another issue of the basic LBP is its sensitivity to noise. Extending upon the binary encoding, a descriptor known as Local Ternary Pattern (LTP) was proposed in [4] to increase the robustness. In the same year, Local Directional Pattern (LDP), which has more discriminant power, was proposed for face recognition in [5]. In a comparative study [6] (2017), the Median Robust Extended Local Binary Pattern (MRELBP) proposed in [7] outperforms 32 other variants and 8 CNN-based methods.

Since then, more LBP variants have been proposed and have demonstrated both effectiveness and computational efficiency. For instance, inspired by LTP and LDP, a method known as Local Directional Ternary Pattern (LDTP) was proposed in [8] (2018). Additionally, in [9] (2019), El-merabet et al. proposed Attractive-and-Repulsive Center-Symmetric Local Binary Patterns (ARCSLBP). ARCSLBP is inspired by CSLBP proposed in [10]. It achieves top performance on 13 datasets when compared against 76 other methods, including 3 deep learning feature extraction methods. Other novel LBP-related texture classification methods include Robust Adaptive Median Binary Pattern (RAMBP) in [11] (2019) and Local Grouped Order and Non-Local Binary Pattern (LGONBP) in [12] (2020). Novel LBP-based methods targeting facial analysis have also been proposed very recently, such as in [13] (2021) and [14] (2021).

3 Methods

3.1 Preliminaries

For each pixel at position (i, j) in the input image, we consider the ordered neighbourhood $\mathcal{N}$ as defined by Eq. 1. There are eight possible starting positions for p_0 and two possible directions for index increments. This study uses, by default, clockwise rotation starting from the top-left pixel.

$$\mathcal{N}_{(i,j)} = \begin{bmatrix} p_0 & p_1 & p_2 \\ p_7 & p_c & p_3 \\ p_6 & p_5 & p_4 \end{bmatrix} \tag{1}$$

The first step of LBP variants is to create an encoding for each 3×3 patch. For this purpose, we define two step functions γ_τ (Eq. 2) and $\bar{\gamma}_\tau$ (Eq. 3) which are used throughout the paper. For brevity, γ is equivalent to $\gamma_{\tau=0}$.

$$\gamma_\tau(p, p_{\text{ref}}) = \begin{cases} 1, & p \geq p_{\text{ref}} + \tau \\ 0, & \text{otherwise} \end{cases} \tag{2}$$

$$\bar{\gamma}_\tau(p, p_{\text{ref}}) = \begin{cases} 1, & p \leq p_{\text{ref}} - \tau \\ 0, & \text{otherwise} \end{cases} \tag{3}$$

After encoding $\mathcal{N}_(i, j)$, the second step is to convert the encoded patch into a single value by a weighted sum.

• *S. Li is with the Department of Computer Science, University of Toronto.*

The result is taken as the value at the corresponding pixel position (i, j) of the output image.

Lastly, the output image is converted to a feature vector to prepare for classification. The convention is to use the histogram distribution of the values. For brevity, we use $\mathbf{hist}_f^d$ to denote the d-dimensional feature vector constructed by applying an operator f to each image pixel and counting the number of occurrences of values in $\{0, ..., d-1\}$.

3.2 LBP

Local Binary Pattern (LBP) proposed by Ojala et el. in [2] aims to characterize the local spatial pattern and contrast in grayscale images. The corresponding value at (i, j) in the LBP image is then computed using Eq. 4.

$$\mathrm{LBP}_{(i,j)} = \sum_{k=0}^{7} \gamma(p_k, p_c) \times 2^k \tag{4}$$

where p_k and p_c are as defined by Eq. 1. Fig. 1 illustrates a simple example of computing LBP values.

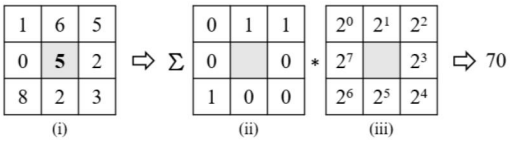

Fig. 1. An example of LBP operator. For each pixel, its eight neighbours (i) are converted into binary code (ii) by comparing their intensities with the central pixel intensity. The code is multiplied by the weight (iii), resulting in a final value of $70 = 2 + 4 + 64$.

The LBP weight vector has its components defined as powers of 2 where the exponent corresponds to the pixel location. There are 256 possible values, ranging from 0 to 255. Thus, for each texture image, we can extract a feature vector $\mathbf{hist}_{\mathrm{LBP}}^{256}$. The feature vector is gray-level invariant and thus robust to illumination change.

3.3 LBP^{ri}

Ojala et al. later introduced the rotation-invariant LBP^{ri} in [3]. As mentioned in section 3.1, there are eight possible starting positions for ordering the neighbours. Each different definition results in a different LBP value. Hence, LBP^{ri} takes the minimum over the eight possible LBP values. The resulting feature vector is similarly 256-dimensional.

3.4 LTP

To improve noise robustness, Local Ternary Pattern (LTP) [4] proposes to use γ_τ and $\bar{\gamma}_\tau$ with $\tau \neq 0$. For each patch at (i, j), LTP constructs two values using Eq. 5 and 6.

$$\mathrm{LTP}_{\mathrm{upper}(i,j)} = \sum_{k=0}^{7} \gamma_\tau(p_k, p_c) \times 2^k \tag{5}$$

$$\mathrm{LTP}_{\mathrm{lower}(i,j)} = \sum_{k=0}^{7} \gamma_\tau(p_k, p_c) \times 2^k \tag{6}$$

The LTP feature is $\mathbf{hist}_{\mathrm{LTP}}^{512} := [\mathbf{hist}_{\mathrm{LTP}_{\mathrm{upper}}}^{256} \ \mathbf{hist}_{\mathrm{LTP}_{\mathrm{lower}}}^{256}]$.

3.5 LDP

To encode a neighbour at position k in the patch (i, j), Local Directional Pattern (LDP) [5] replaces $\gamma(p_k, p_c)$ by a more sophisticated edge response function ER^k as defined by Eq. 7 where M_{LDP}^k is a mask that rotates based on the index k. Eq. 8 gives definitions of M_{LDP}^0 and M_{LDP}^1, and the masks for other k values are rotated accordingly.

$$\mathrm{ER}^k = \sum \mathcal{N}_{(i,j)} * M_{\mathrm{LDP}}^k \tag{7}$$

$$M_{\mathrm{LDP}}^0 = \begin{bmatrix} 5 & 5 & -3 \\ 5 & 0 & -3 \\ -3 & -3 & -3 \end{bmatrix} \quad M_{\mathrm{LDP}}^1 = \begin{bmatrix} 5 & 5 & 5 \\ -3 & 0 & -3 \\ -3 & -3 & -3 \end{bmatrix} \tag{8}$$

After getting the edge responses, LDP assigns 1 to the neighbours with top-m ER and 0 to all others. The LDP value is then computed using the same weight vector as LBP (Eq. 9), resulting in the feature vector $\mathbf{hist}_{\mathrm{LDP}}^{256}$.

$$\mathrm{LDP}_{(i,j)} = \sum_{k=0}^{7} \mathbb{1}(\mathrm{ER}^k \text{ is in top-}m \text{ of 8 ERs}) \times 2^k \tag{9}$$

3.6 LDTP

Local Directional Ternary Pattern (LDTP) [8] takes a similar approach as LDP of computing edge responses. However, in place of the eight M_{LDP}^k, LDTP uses the eight Frei-Chen masks which are defined in detail by Fig. 6 in [8]. In addition, it computes a response ER_c for p_c using a second-derivative Gaussian mask defined by Eq. 10.

$$M_{\mathrm{LDTP}}^c = \frac{1}{4} * \begin{bmatrix} 1 & -2 & 1 \\ 2 & 4 & 2 \\ 1 & -2 & 1 \end{bmatrix} \tag{10}$$

Similar to LTP, LDTP computes two values (Eq. 11 and 12).

$$\mathrm{LDTP}_{\mathrm{upper}(i,j)} = \sum_{k=0}^{7} \gamma(\mathrm{ER}^k, \mathrm{ER}^c) \times 2^k + \gamma(\mathrm{ER}^c, 0) \times 2^8 \tag{11}$$

$$\mathrm{LDTP}_{\mathrm{lower}(i,j)} = \sum_{k=0}^{7} \bar{\gamma}(\mathrm{ER}^k, \mathrm{ER}^c) \times 2^k + \bar{\gamma}(\mathrm{ER}^c, 0) \times 2^8 \tag{12}$$

The LDTP feature is $\mathbf{hist}_{\mathrm{LTP}}^{1024} := [\mathbf{hist}_{\mathrm{LDTP}_{\mathrm{upper}}}^{512} \ \mathbf{hist}_{\mathrm{LDTP}_{\mathrm{lower}}}^{512}]$.

3.7 CSLBP

Center-Symmetric LBP [10] provides lower-dimensional feature vectors by pairing up the eight neighbours (Eq. 13).

$$\mathrm{CSLBP}_{(i,j)} = \sum_{k=0}^{3} \gamma_\tau(p_k, p_{k+4}) \times 2^k \tag{13}$$

Fig. 2 shows a simple example. This results in $\mathbf{hist}_{\mathrm{CSLBP}}^{16}$.

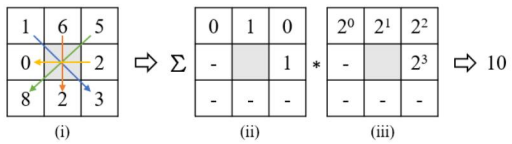

Fig. 2. An example of CSLBP$_{\tau=2}$. The eight neighbours are paired up and the center pixel is not considered (i). The code is created by comparison within each pair (ii) and is multiplied by the weight (iii).

3.8 ARCSLBP

Based on CSLBP, Attractive-Repulsive CSLBP (ARCSLBP) [9] was proposed to characterize attractive and repulsive micro-structures. In particular, ARCSLBP also pairs up the eight neighbours but includes the center pixel in value comparisons. The attractive (A) and repulsive (R) components are defined by Eq. 14 and 15, respectively.

$$A_{(i,j)} = \sum_{k=0}^{3} \gamma(p_k, p_c) \times \gamma(p_{k+4}, p_c) \times 2^k \tag{14}$$

$$R_{(i,j)} = \sum_{k=0}^{3} \bar{\gamma}(p_k, p_c) \times \bar{\gamma}(p_{k+4}, p_c) \times 2^k \tag{15}$$

In brief, a pair has an attractive (repulsive) structure iff both values are greater (smaller) than or equal to the center value.

A major difference between ARCSLBP and the other variants is that it further compares the center pixel with three different statistics: the mean intensity of the image (I_{mean}), the mean intensity of the patch (p_{mean}), and the median intensity of the patch (p_{median}). The complete attractive and repulsive operators are defined by Eq. 16 and 17.

$$\text{ACSLBP}_{(i,j)} = A_{(i,j)} + \begin{bmatrix} \gamma(I_{\text{mean}}, p_c) \\ \gamma(p_{\text{mean}}, p_c) \\ \gamma(p_{\text{median}}, p_c) \end{bmatrix} \cdot \begin{bmatrix} 2^4 \\ 2^5 \\ 2^6 \end{bmatrix} \tag{16}$$

$$\text{RCSLBP}_{(i,j)} = R_{(i,j)} + \begin{bmatrix} \bar{\gamma}(I_{\text{mean}}, p_c) \\ \bar{\gamma}(p_{\text{mean}}, p_c) \\ \bar{\gamma}(p_{\text{median}}, p_c) \end{bmatrix} \cdot \begin{bmatrix} 2^4 \\ 2^5 \\ 2^6 \end{bmatrix} \tag{17}$$

Fig. 3 provides a simple example of the ARCSLBP. The feature vector is $\mathbf{hist}^{256}_{\text{ARCSLBP}} = [\mathbf{hist}^{128}_{\text{ACSLBP}}\ \mathbf{hist}^{128}_{\text{RCSLBP}}]$.

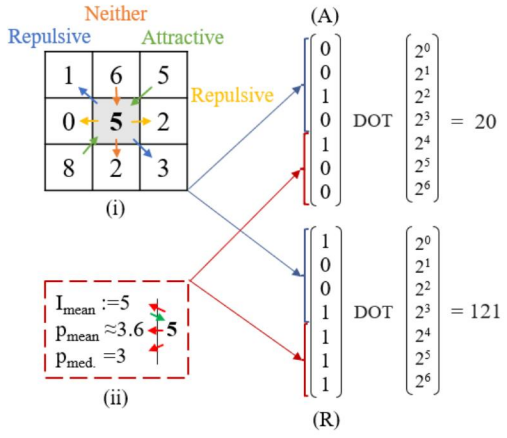

Fig. 3. An example of ARCSLBP. The attractive micro-structure checks if both values in each pair are at least 5 and the repulsive micro-structure checks if both are at most 5 (i). The center pixel is compared with the global mean (I_{mean}), the local mean (p_{mean}) and the local median (p_{median}) (ii). The attractive (A) and the repulsive (R) vectors are obtained by concatenating the two sets of results. The two ARCSLBP values are dot products of the two codes and the weight.

3.9 Proposed Method: ARSBLBP

Inspired by ARCSLBP, this paper proposes Attractive-Repulsive Strength-Based Local Binary Pattern (ARSBLBP). Specifically, ARSBLBP aims to characterize attractive and repulsive micro-structures in a fully rotation-invariant and also more space-efficient way.

While pairing up the neighbours admits some extent of rotation invariance, multiplying the binary codes by different weights eliminates this desired property. In addition, a common shortcoming of the LBP variants is the difficulty of choosing a proper and interpretable ordering of neighbours. Motivated by the above reasons, ARSCLBP measures the overall strength of the local micro-structures by assigning equal weights to the eight comparisons. The 3×3 field is the most attractive (repulsive) iff the center pixel is a local minimum (maximum). Summing over the neighbours results in a range of 0 to 8. To increase the compactness of the encoding, we decrease the value by 1. This is formally defined by Eq. 18 and 19. Each overall strength measure takes on the range of 0 to 7, which is only 3 bits.

$$\text{A}_{\text{strength}(i,j)} = \max\left(0, \sum_{k=0}^{7} \gamma(p_k, p_c) - 1\right) \tag{18}$$

$$\text{R}_{\text{strength}(i,j)} = \max\left(0, \sum_{k=0}^{7} \bar{\gamma}(p_k, p_c) - 1\right) \tag{19}$$

In addition, we also include comparisons between the center pixel and some statistics. In contrast to ARCSLBP which uses both the mean and median of the patch, we only need to consider the local mean. This is because the comparison with the median is already implicitly encoded in the first summation term. Specifically, we know that $\gamma(I_{\text{median}}, p_c) = 1$ if and only if $\sum_{k=0}^{7} \gamma(p_k, p_c) \geq 4$. Hence, we include one comparison with the global mean at the 4^{th} bit and one with the local mean at the 5^{th} bit (Eq. 20 and 21).

$$\text{ASBLBP}_{(i,j)} = \text{A}_{\text{strength}(i,j)} + \begin{bmatrix} \gamma(I_{\text{mean}}, p_c) \\ \gamma(p_{\text{mean}}, p_c) \end{bmatrix} \cdot \begin{bmatrix} 2^3 \\ 2^4 \end{bmatrix} \tag{20}$$

$$\text{RSBLBP}_{(i,j)} = \text{R}_{\text{strength}(i,j)} + \begin{bmatrix} \bar{\gamma}(I_{\text{mean}}, p_c) \\ \bar{\gamma}(p_{\text{mean}}, p_c) \end{bmatrix} \cdot \begin{bmatrix} 2^3 \\ 2^4 \end{bmatrix} \tag{21}$$

Combining the two, we obtain a lower-dimensional feature vector $\mathbf{hist}^{64}_{\text{ARSBLBP}} = [\mathbf{hist}^{32}_{\text{ASBLBP}}\ \mathbf{hist}^{32}_{\text{RSBLBP}}]$. Fig. 4 illustrates the proposed method by an example that can be used to compare and contrast with Fig. 3.

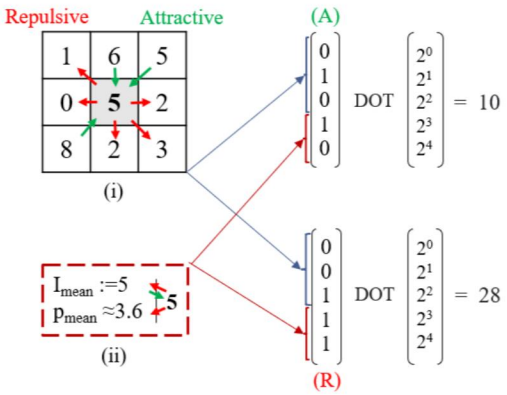

Fig. 4. An example of ARSBLBP. Each neighbour is compared with the center pixel (i) and the center pixel is also compared with the global mean and the local mean (ii). The strength is 3-1=2 (or 010 in binary) for the attractive structure and 5-1=4 (or 100 in binary) for the repulsive.

TABLE 1
The classification accuracy (%) of the eight LBP variants on the four datasets with different characteristics, numbers of images per class ($N_{i/c}$), and numbers of classes (N_c). The best score(s) in each row are highlighted in bold .

	Characteristics	$N_{i/c}$	N_c	LBP	LBP^{ri}	LTP	LDP	LDTP	CSLBP	ARCSLBP	ARSBLBP
USC	Standard	16	13	99.0	93.3	**100.0**	93.3	**100.0**	94.2	**100.0**	**100.0**
USC rot.	7 rotation angles per class	7	13	47.8	95.7	45.7	19.6	58.7	17.4	84.8	**100.0**
Brodatz	Large intra-class variation	25	112	87.9	83.4	88.1	75.1	91.4	72.1	**92.3**	90.1
UIUC	Rotation, scaling, viewpoints	40	25	52.8	51.2	60.0	36.8	58.8	42.0	69.0	**77.0**
Average	————	—	—	71.9	80.9	73.4	56.2	77.2	56.4	86.5	**91.8**

4 Evaluation

4.1 Datasets

To evaluate the methods, we use four datasets with different characteristics, as summarized in Table 1. Each dataset is partitioned into train and test sets of equal sizes.

4.1.1 USC-SIPI

The USC-SIPI (University of Southern California – Signal and Image Processing Institute) dataset includes 13 512×512 images, one for each class. We split each into 16 smaller ones of 128×128 and place 8 of them in the test set. This standard dataset, as shown in Fig. 5, serves as a basic evaluation.

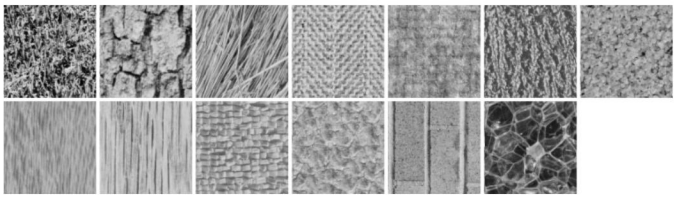

Fig. 5. A 128×128 sample for each of the 13 classes in the USC dataset.

4.1.2 USC-SIPI Rotated

To check rotation invariance, the USC Rotated dataset includes 7 different angles for each of its 13 classes, for a total of 91 images of size 512×512. Fig. 6 shows the seven angles.

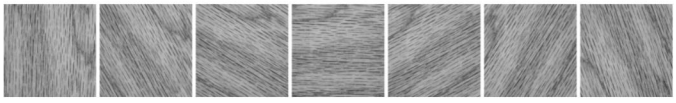

Fig. 6. Seven *weave* images at $\{0, 30, 60, 90, 120, 150, 200\}$ degrees.

4.1.3 Brodatz

The Brodatz dataset consists of 112 640×640 images, one per class. We split each into 25 images of 128×128. Fig. 7 shows its significantly more intra-class variations and inter-class similarity, which makes it more challenging.

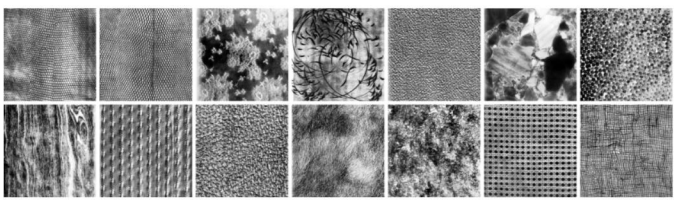

Fig. 7. Sample images of size 640×640 in the Brodatz dataset.

4.1.4 UIUC

The University of Illinois Urbana Champaign (UIUC) texture dataset consists of 1000 256×256 images, divided into 25 classes with 40 images for each. This is the most challenging dataset of the four, with significant variations in scales, angles, and viewpoints. As shown in Fig. 8, the patterns between different classes may also be very similar.

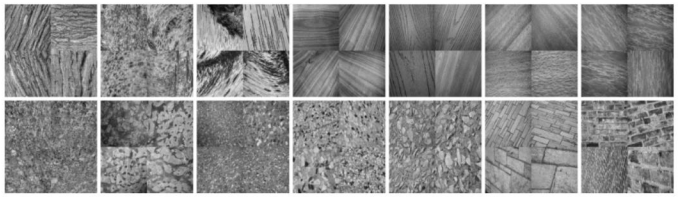

Fig. 8. Four sample images for 14 random classes in the UIUC dataset.

4.2 Classifier

A classifier is required to associate the features with the class labels. Since the focus of this study is the extracted features, we use a simple 1-Nearest-Neighbour classifier.

4.3 Hyperparameters

The only hyperparameters involved are τ for LTP and CSLBP and k for LDP. Following the suggestions in the published papers, we set $\tau = 2$ and $k = 3$.

5 Experimental Results

Table 1 summarizes the classification accuracy for each dataset-method combination. Overall, the proposed ARSBLBP method achieves the best performance for three of the four datasets and also the best on average.

In detail, ARSBLBP achieves 100% accuracy for both the standard USC and the USC Rotated datasets. In comparison, none of the other LBP variants are able to perform very well on both of the datasets. For instance, LBP^{ri} achieves the second-best performance on the rotational dataset but the worst performance on the standard USC dataset.

As for the more challenging Brodatz dataset, the ARCSLBP variant shows the best performance, followed by LDTP and ARSBLBP. More importantly, for the UIUC dataset with a variety of large variations, the proposed ARSBLBP also performs the best, achieving 8% higher than the second best which is ARCSLBP. Overall, it is the only method with an average classification accuracy above 90%.

In addition, we also report the costs of the experiments. Fig. 9 compares the average testing performance with the time and space costs of different LBP variants.

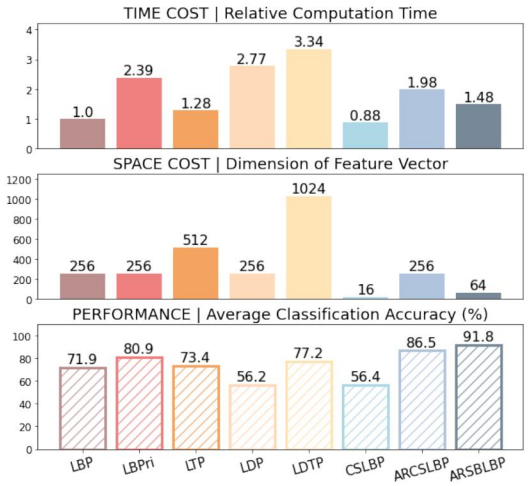

Fig. 9. The trade-off between costs and performance. The time cost of each method is relative to that of LBP.

6 Discussion

Firstly, based on Table 1, the proposed ARSBLBP is the only variant achieving 100% classification scores on both USC standard and rotated datasets. None of the other LBP variants proves to fully rotation-invariant, including LBP^{ri}. LBP^{ri} is only able to consider the eight different angles corresponding to the different starting points. LBP^{ri} also makes compromise on regular datasets, as suggested by its least competitive performance on the USC dataset. ARCSLBP is moderately robust to rotations with a score of 84.8%. Comparatively, the proposed method effectively resolves rotational issues while making no compromise to its discriminant power on rotation-free datasets.

As expected, the classification scores for the most challenging UIUC dataset are significantly lower than all others. Comparing across the methods, the proposed ARSBLBP achieves 8% better than the second best and 17% than the third best. One possible reason is that in a situation with large variations, it is more beneficial to capture coarser patterns. In particular, the better-performing ARCSLBP and ARSBLBP both place more emphasis (i.e. higher weights) on the comparisons between the central pixel and the statistics. These more general and more robust comparisons contribute the most to the resulting values.

For complimentary analysis, Fig. 10 illustrates some qualitative results from LBP, ARCSLBP, and ARSBLBP.

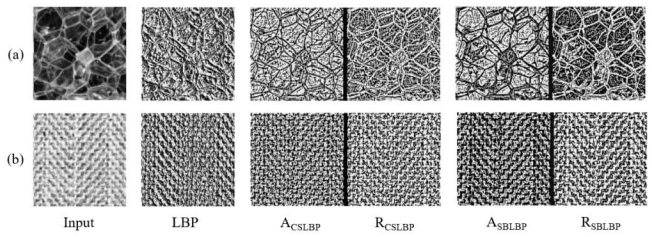

Fig. 10. The image outputs from LBP, ARCSLBP, and ARSBLBP for two sample inputs of herringbone weave (a) and plastic bubbles (b).

In the first case of plastic bubbles, applying the LBP operator is able to capture all edges of the input image. Meanwhile, it also captures many fine details in between the main edges. The magnitudes of the LBP values in the darker gap regions and the lighter regions cover a similar range. In contrast, the separated outputs from ARCSLBP and ARSBLBP clearly illustrate different effects depending on the types of region. The attractive structure assigns larger values to the dark regions whereas the repulsive structure assigns larger values to the brighter regions. This effect is attributable to the comparison with the image mean. The effect is more obvious in the ARSBLBP outputs. This is because the comparison with the image mean is at the second-highest bit for ARSBLBP and the third-highest bit for ARCSLBP.

The second input of herringbone weave has more regular and repeated patterns. This case illustrates how LBP responds to rotations. In particular, we observe different LBP patterns between the lines going downwards and the lines going upwards. The linear structure is preserved in the LBP image for the former but not the latter. In comparison, the proposed ARSBLBP preserves the linear structure for both directions while ARCSLBP preserves the structure for neither.

We recognize that ARSBLBP may not always work. For instance, Fig. 11 shows the responses of ARSBLBP in challenging scenarios with large inter-class similarities and intra-class variations. It is arguably difficult to classify these images correctly even by visual inspection. ARSBLBP performs very well in one case and fails in the other.

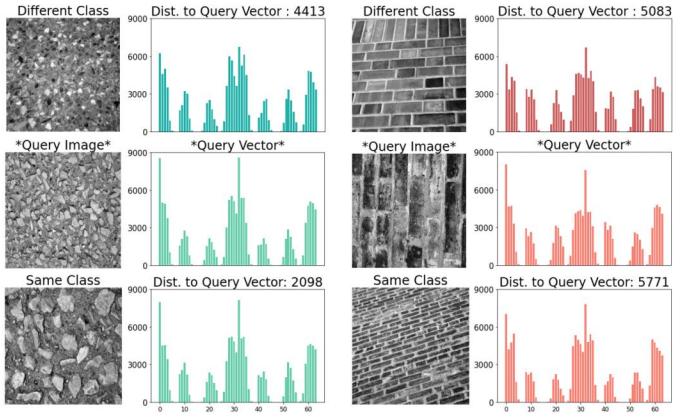

Fig. 11. Some feature vectors constructed by ARSBLBP in cases where there is a great inter-class similarity (between the top and the middle inputs) and a great intra-class variation (between the middle and the bottom inputs). The left is a successful example where the query vector is closer to the one of the same class. The right is a failed example where the query vector is closer to the one of the different class.

Lastly, based on Fig. 9, while showing the best performance, the proposed method is also very efficient in terms of its cost in space. In terms of computation times, it takes longer to construct ARSBLBP feature vectors than LBP, LTP, and CSLBP. Nonetheless, in comparison to the second and the third best-performing methods, ARSBLBP has much lower computational costs in both time and space, achieving a significantly better trade-off between performance and costs.

7 Conclusion

In conclusion, this paper proposes Attractive-Repulsive Strength-Based Local Binary Pattern (ARSBLBP) for textural feature extraction and classification.

The method has been evaluated and compared with seven other classic and novel variants of Local Binary Pattern. Based on four datasets of various characteristics, ARSBLBP achieves the best average classification score on the testing sets. It proves to be fully rotation-invariant and has a comparatively high tolerance level for different forms of variations.

Additionally, its computational time cost is below-average. Its feature vector is only 64-dimensional, which is significantly more space-efficient than the other variants with at least 256-dimensional features.

To further improve the performance, possible future directions include the combination of statistical methods and deep learning methods. For instance, a number of studies such as [15] and [16] have proposed to use LBP images as inputs to CNNs for the purpose of face recognition.

Lastly, we would like to note that in situations with limited training data, traditional methods may be necessary and helpful. Despite the fast development of CNNs, the LBP operator and its variants are still relevant today and can provide promising results with minimal computational resources.

8 Limitations

Limitations exist in the evaluation of the studied methods. For instance, each image in all four datasets consists of a single texture. In practice, the texture segmentation stage may not be as perfect. Behaviours with combinational, noisy texture images should be investigated. It is possible to draw different conclusions about the methods with different datasets.

In addition, using a 1-Nearest-Neighbour classifier may not necessarily be the best option. The impacts of different classifiers on the methods can also be studied in the future. Also, for consistency across the methods, we did not create validation sets for hyperparameter tuning. Instead, the hyperparameters were set following examples in the original papers.

Meanwhile, we recognize that limitations exist in the proposed ARSBLBP method. Despite outperforming the seven other variants, its classification score on the most challenging UIUC dataset is still below 80%. In this case, it may be beneficial to introduce some deep learning techniques. Alternatively, image pre-processing techniques such as perspective correction could be applied prior to LBP operators.

Acknowledgments

The author would like to thank Professor David Lindell, Mian Wei, Parsa Mirdehghan, Shayan Shekarforoush, and Robin Swanson for all their help and support.

References

[1] L. Armi and S. Fekri-Ershad, "Texture image analysis and texture classification methods-a review," *arXiv preprint arXiv:1904.06554*, 2019.

[2] T. Ojala, M. Pietikäinen, and D. Harwood, "A comparative study of texture measures with classification based on featured distributions," *Pattern recognition*, vol. 29, no. 1, pp. 51–59, 1996.

[3] T. Ojala, M. Pietikainen, and T. Maenpaa, "Multiresolution gray-scale and rotation invariant texture classification with local binary patterns," *IEEE Transactions on pattern analysis and machine intelligence*, vol. 24, no. 7, pp. 971–987, 2002.

[4] X. Tan and B. Triggs, "Enhanced local texture feature sets for face recognition under difficult lighting conditions," *IEEE transactions on image processing*, vol. 19, no. 6, pp. 1635–1650, 2010.

[5] T. Jabid, M. H. Kabir, and O. Chae, "Local directional pattern (ldp) for face recognition," in *2010 digest of technical papers international conference on consumer electronics (ICCE)*. IEEE, 2010, pp. 329–330.

[6] L. Liu, P. Fieguth, Y. Guo, X. Wang, and M. Pietikäinen, "Local binary features for texture classification: Taxonomy and experimental study," *Pattern Recognition*, vol. 62, pp. 135–160, 2017.

[7] L. Liu, S. Lao, P. W. Fieguth, Y. Guo, X. Wang, and M. Pietikäinen, "Median robust extended local binary pattern for texture classification," *IEEE Transactions on Image Processing*, vol. 25, no. 3, pp. 1368–1381, 2016.

[8] I. El khadiri, A. Chahi, Y. El merabet, Y. Ruichek, and R. Touahni, "Local directional ternary pattern: A new texture descriptor for texture classification," *Computer vision and image understanding*, vol. 169, pp. 14–27, 2018.

[9] Y. El merabet, Y. Ruichek, and A. El idrissi, "Attractive-and-repulsive center-symmetric local binary patterns for texture classification," *Engineering Applications of Artificial Intelligence*, vol. 78, pp. 158–172, 2019.

[10] M. Heikkilä, M. Pietikäinen, and C. Schmid, "Description of interest regions with center-symmetric local binary patterns," in *Computer vision, graphics and image processing*. Springer, 2006, pp. 58–69.

[11] M. Alkhatib and A. Hafiane, "Robust adaptive median binary pattern for noisy texture classification and retrieval," *IEEE Transactions on Image Processing*, vol. 28, no. 11, pp. 5407–5418, 2019.

[12] T. Song, J. Feng, L. Luo, C. Gao, and H. Li, "Robust texture description using local grouped order pattern and non-local binary pattern," *IEEE Transactions on Circuits and Systems for Video Technology*, vol. 31, no. 1, pp. 189–202, 2020.

[13] S. Karanwal and M. Diwakar, "Od-lbp: Orthogonal difference-local binary pattern for face recognition," *Digital Signal Processing*, vol. 110, p. 102948, 2021.

[14] D. G. R. Kola and S. K. Samayamantula, "A novel approach for facial expression recognition using local binary pattern with adaptive window," *Multimedia Tools and Applications*, vol. 80, no. 2, pp. 2243–2262, 2021.

[15] H. Zhang, Z. Qu, L. Yuan, and G. Li, "A face recognition method based on lbp feature for cnn," in *2017 IEEE 2nd Advanced Information Technology, Electronic and Automation Control Conference (IAEAC)*. IEEE, 2017, pp. 544–547.

[16] P. Ke, M. Cai, H. Wang, and J. Chen, "A novel face recognition algorithm based on the combination of lbp and cnn," in *2018 14th IEEE International Conference on Signal Processing (ICSP)*. IEEE, 2018, pp. 539–543.